Structural and Multidisciplinary Optimization (2021) 64:2449–2464
https://doi.org/10.1007/s00158-021-02999-9

RESEARCH PAPER

An efficient decoupled method for time-variant reliability-based design optimization

Yunwei Zhang [1] · Chunlin Gong [1] · Chunna Li [1] · Hai Fang [2]

Received: 9 February 2021 / Revised: 25 May 2021 / Accepted: 22 June 2021 / Published online: 5 August 2021

Abstract

Time-variant reliability-based design optimization (tRBDO) can rationally consider the time-variant uncertainties in engineering structures and find the optimal design that can keep reliable throughout its whole life cycle. However, solving the tRBDO involves a nested double-loop procedure and requires excessive computational cost. In this paper, a novel decoupled method called sequential approximate time-variant reliability analysis and optimization (SATO) is proposed to improve the efficiency of tRBDO. First, a two-step method is proposed to transform the original tRBDO problem into an equivalent deterministic optimization problem according to the results of time-variant reliability analysis (TRA). Second, a novel approximate TRA (ATRA) method based the least-square method is proposed to reduce the computational cost of TRA. Finally, the proposed SATO method decouples the original double-loop procedure in tRBDO into a sequential process of ATRA and deterministic optimization. Test results of a complicated welded beam problem verify that the proposed method can achieve similar accuracy and much higher efficiency than the compared methods. A rocket inter-stage structure problem demonstrates the capability of the proposed method in practical engineering applications.

Keywords Time-variant uncertainty · Time-variant reliability-based design optimization · Decoupled method · Stochastic process · Most probable point

1 Introduction

Uncertainties, such as material properties, geometrical sizes, and external loads, are ubiquitous in practical engineering structures. Reliability-based design optimization (RBDO) can rationally account for the uncertainties in the optimization process and find the optimal solution satisfying reliability requirements. However, directly solving the RBDO involves a nested double-loop procedure (Tu et al. 1999; Schuëller and Jensen 2008), in which the outer loop updates the design point, and the inner loop analyzes whether the reliability constraints are satisfied. This nested procedure needs excessive computational cost, especially when computationally expensive simulation models are involved. In recent decades, many RBDO methods, including the decoupled methods and single-loop methods, have been proposed to improve the efficiency. The decoupled methods (Du and Chen 2004; Yi et al. 2016; Huang et al. 2016; Li et al. 2019) separate the inner reliability-analysis loop from the outer optimization loop to avoid the nested procedure. The sequential optimization and reliability assessment (SORA) (Du and Chen 2004) is one of the most representative decoupled **RBDO** methods. The single-loop methods (Liang et al. 2004; Agarwal et al. 2007; Lim and Lee 2016; Ren et al. 2021) directly remove the inner reliability-analysis loop by transforming reliability constraints into equivalent deterministic constraints, which are suitable for linear or weakly nonlinear problems (Yi et al. 2016).

In addition to the time-independent uncertainties, practical engineering structures are also affected by various dynamic or time-variant uncertainties (Li and Wang 2017; Yu et al. 2019; Zafar and Wang 2020), such as material deterioration and load fluctuation. However, these time-variant uncertainties cannot

Responsible Editor: Tae Hee Lee

✉ Chunlin Gong
leonwood@nwpu.edu.cn

[1] Shaanxi Aerospace Flight Vehicle Design Key Laboratory, School of Astronautics, Northwestern Polytechnical University, Xi'an 710072, China

[2] Shanghai Electro-Mechanical Engineering Institute, Shanghai 201109, China

be considered in conventional static RBDO methods. Under these time-variant uncertainties, the reliability of the structure is no longer a constant, but varies with time. To ensure the safety of the structure throughout its whole life cycle, time-variant reliability requirements need to be included in the RBDO formulation as constraints, which leads to the time-variant RBDO (tRBDO) (Wang and Wang 2012; Wang et al. 2014). Similar to RBDO, directly solving tRBDO also involves a nested double-loop procedure, i.e., the inner loop for time-variant reliability analysis (TRA) (Jiang et al. 2020; Yu et al. 2020) and the outer loop for updating the design point. However, the solution process of tRBDO is far more complicated and time-consuming than that of the conventional static RBDO.

In recent years, tRBDO has become a frontier research direction and attracted increasing attention in the field of structure reliability (Jiang et al. 2017). Inspired by the success of decoupled static RBDO methods, some decoupled tRBDO methods have also been developed. Hu and Du (Hu and Du 2016) extended the classical SORA to solve tRBDO problems with stationary stochastic loads, but it cannot deal with more general tRBDO problems with non-stationary stochastic processes. Huang et al. (Huang et al. 2017) proposed a single-loop approach, which discretizes the time-variant reliability constraints into many time-independent ones, and transforms the nested tRBDO into an iterative process of TRA, constraint discretization, and conventional RBDO. Jiang et al. (Jiang et al. 2017) developed a general framework called time-invariant equivalent method (TIEM) to decouple the tRBDO into a sequence of cycles of TRA and conventional RBDO at the initial time instant. Fang et al. (Fang et al. 2019) introduced the concept of equivalent most probable point (EMPP), with which the tRBDO is transformed into an equivalent time-independent RBDO. Shi et al. (Shi et al. 2020) developed a two-step method to improve the efficiency of tRBDO, in which the first step aims to make the minimum instantaneous reliability index of the constraint satisfy the reliability index target, and the second step performs TRA and deterministic optimization. Some other tRBDO methods can be found in Refs. (Hawchar et al. 2018; Li and Wang 2018; Zafar et al. 2020).

Although some decoupled methods have been developed, solving the tRBDO efficiently is still a major challenge. The reasons are at least twofold. First, most of the existing decoupled tRBDO methods try to transform the tRBDO problem into an equivalent static RBDO problem. However, as mentioned above, solving the static RBDO itself is still extremely time-consuming, let alone further embedding it into a sequential optimization process. Second, the TRA process, as an essential sub-procedure of tRBDO, is computationally expensive and must be frequently **invoked. Jiang et al.** (Jiang et al. 2017) **pointed out that** most of the computational costs for solving the tRBDO are actually spent on the repeated TRA invocations.

This paper aims to address the above two problems and improve the efficiency of tRBDO. A novel decoupled method called Sequential Approximate TRA and Optimization (SATO) is proposed. First, according to the TRA results, the original tRBDO problem is directly transformed into an equivalent deterministic optimization problem, instead of a static RBDO problem, hence avoiding repeatedly solving the static RBDO problems. Second, a novel approximate TRA (ATRA) method based on least-square method is proposed, which can efficiently calculate the time-variant reliability. Finally, the double-loop nested procedure in the original tRBDO is decoupled into a sequential process of ATRA and deterministic optimization. The proposed SATO method can simplify the solution process and significantly improve the efficiency of tRBDO.

The rest of this paper is organized as follows. Section 2 presents the formulation of the tRBDO problem. Section 3 describes the proposed SATO method in detail. Afterwards, the validation and application of the proposed method are presented in Section 4, and conclusions of this paper are finally given in Section 5.

2 Formulation of the tRBDO problem

Under various time-variant uncertainties, the general time-variant performance function of a structure can be expressed as $g(\boldsymbol{X},\boldsymbol{Y}(t),t)$, where $\mathbf{X}$ is a n_x-dimensional vector of random variables, $\mathbf{Y}(t)$ is a n_Y-dimensional vector of stochastic processes, and $_t$ is the time parameter within the time interval of interest $[0,T]$. $g(\boldsymbol{X},\boldsymbol{Y}(t),t) < 0$ indicates the safe state of the structure. Accordingly, the safety region SR can be defined as the set of the input vectors $[\mathbf{X},\mathbf{Y}(t)]$ satisfying $g(\mathbf{X},\mathbf{Y}(t),t) <0$ for $t \in[0,T]$, which can be expressed as

$$SR = \{[\mathbf{X}, \mathbf{Y}(t)] | g(\mathbf{X}, \mathbf{Y}(t), t) < 0, \nabla t \in [0, T]\} \tag{1}$$

Then, we can define an indicator function $I_{sr}(\mathbf{X},\mathbf{Y}(t))$ based on whether the point $[\mathbf{X},\mathbf{Y}(t)]$ is in the safety region (Wei et al. 2017):

$$I_{SR}(\mathbf{X}, \mathbf{Y}(t)) = \begin{cases} 1 & [\mathbf{X}, \mathbf{Y}(t)] \in SR \\ 0 & [\mathbf{X}, \mathbf{Y}(t)] \notin SR \end{cases} \tag{2}$$

The aim of TRA is to calculate the probability that the structure remains in safe state over the time interval $[0, T]$, which can be formulated as

$$\begin{aligned} P(T) &= \Pr\{g(\mathbf{X}, \mathbf{Y}(t), t) < 0, \forall t \in [0, T]\} \\ &= E[I_{SR}(\mathbf{X}, \mathbf{Y}(t))] \end{aligned} \tag{3}$$

where $\Pr\{\square\}$ denotes the probability operator, and it can be defined as the mathematical expectation of the indicator function $I_{SR}(\mathbf{X}, \mathbf{Y}(t))$ (Wang et al. 2017).

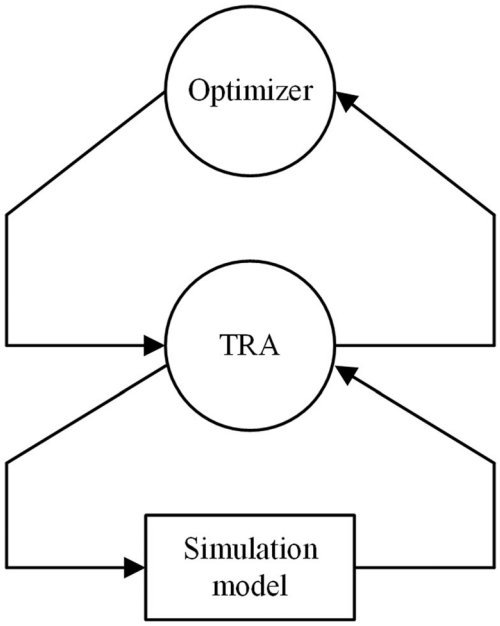

Fig. 1 Double-loop nested procedure in tRBDO

In practice, the time-variant reliability index β is often used to measure the time-variant reliability, which is calculated by

$$\beta = \Phi^{-1}(P(T)) \tag{4}$$

where $\Phi(\square)$ is the standard normal cumulative distribution function.

The tRBDO treats the time-variant reliability as constraint in the optimization formulation, which is expressed as

$$\begin{aligned} &\text{find} && \mathbf{d}, \boldsymbol{\mu}_Z \\ &\min && f(\mathbf{d}, \boldsymbol{\mu}_\mathbf{Z}, \boldsymbol{\mu}_\mathbf{P}) \\ &s.t. && P(t_s, t_e) = \Pr\{\mathrm{g}(\mathbf{d}, \mathbf{X}, \mathbf{Y}(t), t) < 0, \forall t \in [0, T]\} > \Phi(\beta_{\mathrm{tar}}) \\ & && \mathbf{X} = [\mathbf{Z}, \mathbf{P}], \mathbf{d}^L \le \mathbf{d} \le^U, \boldsymbol{\mu}_Z^L \le \boldsymbol{\mu}_z \le \boldsymbol{\mu}_Z^U \end{aligned} \tag{5}$$

where $_f$ is the objective function;β_{tar} is the target time-variant reliability index of the performance function g(**d**, ***X***, ***Y***(*t*),*t*), **d** denotes a n_d-dimensional deterministic design vector with the lower bound $\mathbf{d}^L$ and upper bound $\mathbf{d}^U$; $_\mathbf{Z}$ denotes a n_z-dimensional random design vector; $\boldsymbol{\mu}_\mathbf{Z}$ denotes the mean vector of **Z** with the lower bound $\boldsymbol{\mu}_\mathbf{Z}^L$ and upper bound $\boldsymbol{\mu}_\mathbf{Z}^U$; and **P** represents a n_P-dimensional random parameter vector with the mean vector $\boldsymbol{\mu}_\mathbf{P}$.

It can be noticed from (5) that the tRBDO originally involves a double-loop nested procedure, as depicted in Fig. 1. The inner TRA loop is repeatedly invoked by the outer optimization loop. Due to the low efficiency of the TRA itself and the large number of required TRA invocations, it is a huge challenge to efficiently solve the tRBDO problem.

3 The proposed SATO method

The proposed SATO method decouples the nested procedure in tRBDO into two main sub-procedures: deterministic optimization and approximate TRA. The detailed process is presented as follows.

3.1 Construction of the equivalent deterministic optimization

First, a novel TRA method based on approximating the MPP trajectory (AMPPT) (Zhang et al. 2021) is performed at the initial design point $[\mathbf{d}^{(1)}, \boldsymbol{\mu}_\mathbf{Z}^{(1)}]$. The AMPPT method can not only calculate the time-variant reliability index β_{cur}, but also identify the critical time instants within [0, *T*] and the corresponding MPPs $\{(t_i, \mathbf{u}_{\mathrm{MPP}}(t_i)) | i = 1, 2, \ldots, n_t\}$ through an adaptive sampling process. The AMPPT method is briefly described in the Appendix.

Then, according to the TRA results of the AMPPT method, this subsection proposes a two-step method to transform the original time-variant reliability constraint into a deterministic one, and correspondingly constructs an equivalent deterministic optimization problem for the original tRBDO problem.

3.1.1 First transformation of the time-variant reliability constraint

For an arbitrary critical time instant t_i from the time-MPP pairs $\{(t_i, \mathbf{u}_{\mathrm{MPP}}(t_i)) | i = 1, 2, \ldots, n_t\}$ obtained by AMPPT, we can calculate the instantaneous reliability index $\beta(t_i)$ at t_i as

$$\Phi^{-1}(\Pr\{g(\mathbf{d}, \mathbf{X}, \mathbf{Y}(t_i), t_i) < 0\}) = \beta(t_i) = \|\mathbf{u}_{\mathrm{MPP}}(t_i)\| \tag{6}$$

If the original time-variant reliability constraint $P(T) = \Pr\{g(\mathbf{d}, \mathbf{X}, \mathbf{Y}(t), t) < 0, \forall t \in [0, T]\} > \Phi(\beta_{\mathrm{tar}})$ in (5) is satisfied, the following inequality must hold:

$$0 > \beta_{\mathrm{tar}} - \beta_{\mathrm{cur}} \tag{7}$$

Then, add $\Phi^{-1}(\Pr\{g(\mathbf{d}, \mathbf{X}, \mathbf{Y}(t_i), t_i) < 0\})$ and $\beta(t_i)$ to the left and right side of (7), respectively, and we can obtain

$$\Pr\{g(\mathbf{d}, \mathbf{X}, \mathbf{Y}(t), t) < 0\} > \Phi(\beta_{\mathrm{tar}} - \beta_{\mathrm{cur}} + \beta(t_i)) \tag{8}$$

For clarity, (8) can be further rewritten as

$$\begin{aligned} &\Pr\{g_{t_i}(\mathbf{M}) < 0\} > \Phi(\beta_{\mathrm{tar}}(t_i)) \\ &\beta_{\mathrm{tar}}(t_i) = \beta_{\mathrm{tar}} - \beta_{\mathrm{cur}} + \beta(t_i) \end{aligned} \tag{9}$$

where $g_{t_i}(\mathrm{M})$ represents the instantaneous performance function $g(\mathrm{d}, \mathrm{X}, \mathrm{Y}(t_i), t_i)$; $\mathbf{M} = [\mathbf{X}, \mathbf{Y}(t_i)] = [\mathbf{Z}, \mathbf{P}, \mathbf{Y}(t_i)]$ denotes all the random variables; and $\beta_{\mathrm{tar}}(t_i)$ is the target instantaneous reliability index at t_i. Therefore, it can be noticed that the

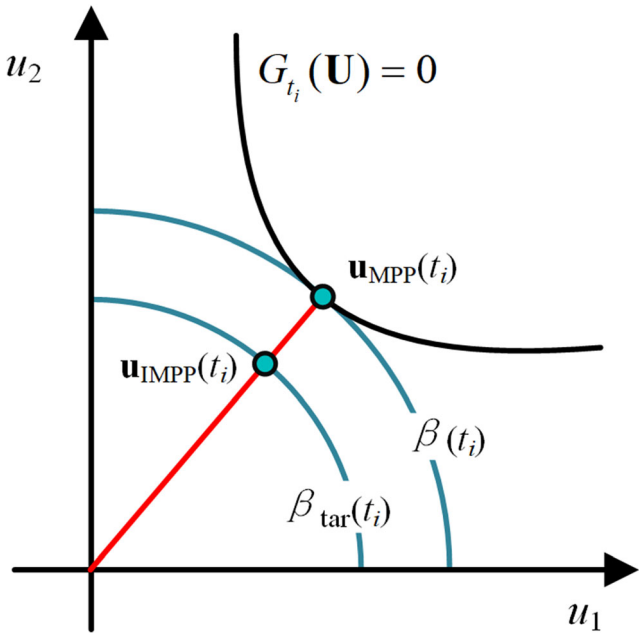

Fig. 2 Schematic diagram of estimating $\mathbf{u}_{\mathrm{IMPP}}(t_i)$

original time-variant reliability constraint is transformed into a single conventional time-independent reliability constraint in (9).

3.1.2 Second transformation of the time-independent reliability constraint

After the first transformation, the performance measure approach (PMA) (Tu et al. 1999; Du and Chen 2004) can be used to further transform (9) into an equivalent deterministic constraint. To this end, the following optimization must be solved to search the inverse MPP (IMPP) $\mathbf{u}_{\mathrm{IMPP}}(t_i)$ corresponding to the target reliability index $\beta_{\mathrm{tar}}(t_i)$

$$\begin{aligned} &\max \quad G_{t_i(\mathbf{u})} \\ &\text{s.t.} \quad \|\mathbf{u}\| = \beta_{\mathrm{tar}}(t_i) \end{aligned} \tag{10}$$

where $G_{t_i}(\mathbf{u})$ represents the transformed performance function of $G_{t_i}(\mathbf{M})$ in u-space.

The advanced mean value (AMV) (Wu et al. 1990) method can be used to solve (10), and its iterative formula is expressed as

$$\mathbf{u}^{(i)} = \beta_{\mathrm{tar}}(t_i)\frac{\nabla G_{t_i(\mathbf{u}^{(j-1)})}}{\left\|\nabla G_{t_i(\mathbf{u}^{(j-1)})}\right\|} \tag{11}$$

However, it is clear from (11) that AMV is a gradient-based algorithm, and in each iteration, it needs to calculate the gradients of $G_{t_i}(\mathbf{u})$, which is computationally expensive. To reduce the computational cost, this paper directly substitutes the MPP $\mathbf{u}_{\mathrm{MPP}}(t_i)$ into (11) to estimate $\mathbf{u}_{\mathrm{MPP}}(t_i)$ as

$$\mathbf{u}_{\mathrm{IMPP}}(t_i) \approx \beta_{\mathrm{tar}}(t_i)\frac{\nabla G_{t_i(\mathbf{u}_{\mathrm{MPP}}(t_i))}}{\left\|\nabla G_{t_i(\mathbf{u}_{\mathrm{MPP}}(t_i))}\right\|} \tag{12}$$

According to the property that the gradient of the instantaneous performance function at the MPP $\nabla G_{t_i}(\mathbf{u}_{\mathrm{MPP}}(t_i))$ is parallel to the MPP $\mathbf{u}_{\mathrm{MPP}}(t_i)$ (Rackwitz and Flessler 1978), we know that

$$\nabla G_{t_i}(\mathbf{u}_{\mathrm{MPP}}(t_i)) = k\mathbf{u}_{\mathrm{MPP}}(t_i) \tag{13}$$

where k is a constant, and $k > 0$.

Then, (12) can be further written as

$$\mathbf{u}_{\mathrm{MPP}}(t_i) \approx \beta_{\mathrm{tar}}(t_i)\frac{k\mathbf{u}_{\mathrm{MPP}}(t_i)}{\|k\mathbf{u}_{\mathrm{MPP}}(t_i)\|} = \frac{\beta_{\mathrm{tar}}(t_i)}{\beta(t_i)}\mathbf{u}_{\mathrm{MPP}}(t_i) \tag{14}$$

This method to estimate $\mathbf{u}_{\mathrm{IMPP}}(t_i)$ is depicted in Fig. 2. This method avoids calculating the gradients $\Delta G_{t_i}(\mathbf{u}_{\mathrm{MPP}}(t_i))$, and does not require any performance function evaluations.

After $\mathbf{u}_{\mathrm{IMPP}}(t_i)$ is obtained, a shifting vector $\mathbf{S}^{(j+1)}$ can be constructed by

$$\begin{aligned} \mathbf{S}^{(j+1)} &= \boldsymbol{\mu}_{\mathbf{M}}^{(j)} - \mathrm{Tr}^{-1}(\mathbf{u}_{\mathrm{IMPP}}(t_i)) \\ &= \left[\boldsymbol{\mu}_{\mathbf{Z}}^{(j)}, \boldsymbol{\mu}_{\mathbf{P}}, \boldsymbol{\mu}_{\mathbf{Y}(t_i)}\right] - \mathrm{Tr}^{-1}\left(\frac{\beta_{\mathrm{tar}}(t_i)}{\beta(t_i)}\mathbf{u}_{\mathrm{MPP}}(t_i)\right) \end{aligned} \tag{15}$$

where $\mathrm{Tr}^{-1}(\bullet)$ denotes the mapping transformation from u-space to the original space, and j represents the iteration counter.

Then, as in SORA (Du and Chen 2004), the time-independent reliability constraint in (9) can be further transformed into an equivalent deterministic constraint as

$$g_{t_i}\left(\boldsymbol{\mu}_{\mathrm{M}} - \mathbf{S}^{(j+1)}\right) < 0 \tag{16}$$

After the above two-step transformation, the original time-variant reliability constraint is converted into a deterministic one. Accordingly, the original tRBDO problem in (5) can be transformed into an equivalent deterministic optimization problem as

$$\begin{aligned} &\text{find} \quad \mathbf{d}, \boldsymbol{\mu}_{\mathrm{Z}} \\ &\min \quad f\left(\mathbf{d}, \boldsymbol{\mu}_{\mathrm{Z}}, \boldsymbol{\mu}_{\mathrm{p}}\right) \\ &\text{s.t.} \quad \mathrm{g}_{t_i}\left(\mu_M - S^{(j+1)}\right) < 0 \\ &\quad \boldsymbol{\mu}_{\mathrm{M}} = \left[\boldsymbol{\mu}_{\mathrm{Z}}, \boldsymbol{\mu}_{\mathrm{p}}, \boldsymbol{\mu}_{Y(t_i)}\right] \\ &\quad \mathbf{d}^L \le \mathbf{d} \le \mathbf{d}^U, \boldsymbol{\mu}_{\mathrm{Z}}^L \le \boldsymbol{\mu}_{\mathrm{Z}} \le \boldsymbol{\mu}_{\mathbf{Z}}^U \end{aligned} \tag{17}$$

Then, (17) can be solved to obtain a new design point $\left[\mathbf{d}^{(j+1)}, \boldsymbol{\mu}_{\mathrm{Z}}^{(j+1)}\right]$ for the next iteration.

3.2 Approximate TRA method based on least-square method

This subsection proposes an efficient ATRA method to calculate the time-variant reliability at the new design point $\left[\mathbf{d}^{(j+1)}, \boldsymbol{\mu}_{\mathrm{Z}}^{(j+1)}\right]$, instead of using the AMPPT method.

3.2.1 The proposed ATRA method

The proposed ATRA method is based on first-order Taylor expansion of the time-variant performance function $g(d, X, Y(t), t)$ and the least-square method. First-order Taylor expansion model has been widely used in static RBDO method, such as the Sequential Approximate Programming (SAP) (Cheng et al. 2006; Yi and Cheng 2008), the Approximate SORA (ASORA) (Yi et al. 2016), and the direct decoupling method (Zou and Mahadevan 2006). However, in tRBDO, the performance function $g(d, X, Y(t), t)$ is a function of time, and it is extremely difficult to directly build the Taylor expansion models of $g(d, X, Y(t), t)$ throughout the whole time interval $[0, T]$. Fortunately, as described in the Appendix, the AMPPT method can identify the critical time instants $t_i (i = 1, 2, \ldots n_t)$, within $[0, T]$. Therefore, it is unnecessary to approximate $g(d, X, Y(t), t)$ over $[0, T]$. Instead, we can only approximate $g(d, X, Y(t), t)$ at these critical time instants, which can significantly alleviate the computational burden in building the Taylor expansion models.

To the describe the dependence of the instantaneous performance function $G_{ti}(\boldsymbol{u})$ in u-space on the design point $[\boldsymbol{d}, \boldsymbol{\mu_z}]$, we rewrite $G_{ti}(\boldsymbol{u})$ as $G_{ti}(\boldsymbol{u}, \boldsymbol{d}, \boldsymbol{\mu_z})$. Then, $G_{ti}(\boldsymbol{u}, \boldsymbol{d}, \boldsymbol{\mu_z})$ can be approximated by first-order Taylor expansion at the point $\left[\boldsymbol{u}_{MPP}^{(j)}(t_i), \boldsymbol{d}^{(j)}, \boldsymbol{\mu}_{\boldsymbol{z}}^{(j)}\right]$, as:

$$G_{t_i}(\mathbf{u}, \mathbf{d}, \boldsymbol{\mu}_{\mathbf{Z}}) \approx G_{t_i}\left(\mathbf{u}_{\mathrm{MPP}}^{(j)}(t_i), \mathbf{d}^{(j)}, \boldsymbol{\mu}_{\mathbf{Z}}^{(j)}\right) + \left[\frac{\partial G_{t_i}\left(\mathbf{u}_{\mathrm{MPP}}^{(j)}(t_i), \mathbf{d}^{(j)}, \boldsymbol{\mu}_{\mathbf{Z}}^{(j)}\right)}{\partial \mathbf{u}}\right]^T \left(\mathbf{u} - \mathbf{u}_{\mathrm{MPP}}^{(j)}(t_i)\right) + \left[\frac{\partial G_{t_i}\left(\mathbf{u}_{\mathrm{MPP}}^{(j)}(t_i), \mathbf{d}^{(j)}, \boldsymbol{\mu}_{\mathbf{Z}}^{(j)}\right)}{\partial \mathbf{d}}\right]^T \left(\mathbf{d} - \mathbf{d}^{(j)}\right) + \left[\frac{\partial G_{t_i}\left(\mathbf{u}_{\mathrm{MPP}}^{(j)}(t_i), \mathbf{d}^{(j)}, \boldsymbol{\mu}_{\mathbf{Z}}^{(j)}\right)}{\partial \boldsymbol{\mu}_{\mathbf{Z}}}\right]^T \left(\boldsymbol{\mu}_{\mathbf{Z}} - \boldsymbol{\mu}_{\mathbf{Z}}^{(j)}\right) \tag{18}$$

where

1) for the first term on the right side of (18), since $\mathbf{u}_{\mathrm{MPP}}^{(j)}(t_i)$ is an MPP, we know that

$$G_{t_i}\left(\mathbf{u}_{\mathrm{MPP}}^{(j)}(t_i), \mathbf{d}^{(j)}, \boldsymbol{\mu}_{\mathbf{Z}}^{(j)}\right) = 0 \tag{19}$$

2) for the second term, $\partial G_{t_i}\left(\mathbf{u}_{\mathrm{MPP}}^{(j)}(t_i), \mathbf{d}^{(j)}, \boldsymbol{\mu}_{\boldsymbol{z}}^{(j)}\right)/\partial \mathbf{u}$ is the partial derivative of $G_{t_i}(u, d, \mu_{\mathrm{Z}})$ with respect to $\mathbf{u}$ at the point $\left[\mathbf{u}_{\mathrm{MPP}}^{(j)}(t_i), d^{(j)}, \boldsymbol{\mu}_{\mathrm{Z}}^{(j)}\right]$, and

$$\partial G_{t_i}\left(\mathbf{u}_{\mathrm{MPP}}^{(j)}(t_i), \mathbf{d}^{(j)}, \boldsymbol{\mu}_{\mathrm{Z}}^{(j)}\right)/\partial \mathbf{u} = k\mathbf{u}_{\mathrm{MPP}}^{(j)}(t_i) \tag{20}$$

3) for the third and the fourth term, $\partial G_{t_i}\left(\mathbf{u}_{\mathrm{MPP}}^{(j)}(t_i), \mathbf{d}^{(j)}, \boldsymbol{\mu}_{\mathrm{Z}}^{(j)}\right)/\partial \mathbf{d}$ and $\partial G_{t_i}\left(\mathbf{u}_{\mathrm{MPP}}^{(j)}(t_i), \mathbf{d}^{(j)}, \mu_{\mathrm{z}}^{(j)}\right)/\partial \boldsymbol{\mu}_{\mathrm{z}}$ are the partial derivative of $G_{t_i}(\mathbf{u}, \mathbf{d}, \boldsymbol{\mu}_{\mathrm{z}})$ with respect to $\mathbf{d}$ and $\boldsymbol{\mu}_{\mathbf{z}}$ respectively at $\left[\mathbf{u}_{\mathrm{MPP}}^{(j)}(t_i), \mathbf{d}^{(j)}, \boldsymbol{\mu}_{\mathbf{z}}^{(j)}\right]$, which can be calculated by numerical method as

$$\begin{aligned} \mathbf{A} &= \frac{\partial G_{t_i}\left(\mathbf{u}_{\mathrm{MPP}}^{(j)}(t_i), \mathbf{d}^{(j)}, \boldsymbol{\mu}_{\mathbf{Z}}^{(j)}\right)}{\partial \mathbf{d}} = \frac{G_{t_i}\left(\mathbf{u}_{\mathrm{MPP}}^{(j)}(t_i), \mathbf{d}^{(j)} + \Delta\mathbf{d}, \boldsymbol{\mu}_{\mathbf{Z}}^{(j)}\right)}{\Delta\mathbf{d}} \\ \mathbf{B} &= \frac{\partial G_{t_i}\left(\mathbf{u}_{\mathrm{MPP}}^{(j)}(t_i), \mathbf{d}^{(j)}, \boldsymbol{\mu}_{\mathbf{Z}}^{(j)}\right)}{\partial \boldsymbol{\mu}_{\mathbf{Z}}} = \frac{G_{t_i}\left(\mathbf{u}_{\mathrm{MPP}}^{(j)}(t_i), \mathbf{d}^{(j)}, \boldsymbol{\mu}_{\mathbf{Z}}^{(j)} + \Delta\boldsymbol{\mu}_{\mathbf{Z}}\right)}{\Delta\boldsymbol{\mu}_{\mathbf{Z}}} \end{aligned} \tag{21}$$

Then, substitute (19)~(21) and the new design point $\left[\mathrm{d}^{(j+1)}, \boldsymbol{\mu}_{\boldsymbol{z}}^{(j+1)}\right]$ into (18), we can obtain the approximated instantaneous performance function at t_i:

$$\begin{aligned} \widehat{G}_{t_i}\left(\mathbf{u}, \mathbf{d}^{(\mathrm{j}+1)}, \boldsymbol{\mu}_{\mathbf{z}}^{(j+1)}\right) &= k\left[\mathbf{u}_{MPP}^{(j)}(t_i)\right]^T\left(\mathbf{u} - \mathbf{u}_{MPP}^{(j)}(t_i)\right) + \mathbf{A}^T\Delta\mathbf{d}^{(j+1)} + \mathbf{B}^T\Delta\boldsymbol{\mu}_{\mathbf{z}}^{(j+1)} \\ &= k\left[\mathbf{u}_{MPP}^{(j)}(t_i)\right]^T\mathbf{u} - k\beta^2 + \mathbf{A}^{\mathrm{T}}\Delta\mathbf{d}^{(j+1)} + \boldsymbol{B}^T\Delta\boldsymbol{\mu}_{\mathbf{Z}}^{(j+1)} \end{aligned} \tag{22}$$

where

$$\begin{aligned} \Delta\mathbf{d}^{(j+1)} &= \mathbf{d}^{(j+1)} - \mathbf{d}^{(1)} \\ \Delta\boldsymbol{\mu}_{\mathrm{z}}^{(j+1)} &= \boldsymbol{\mu}_{\mathrm{Z}}^{(j+1)} - \mathbf{d}_{\mathbf{Z}}^{(j)} \end{aligned} \tag{23}$$

By now, with $\widehat{G}_{t_i}\left(\mathbf{u}, \mathbf{d}^{(\mathrm{j}+1)}, \boldsymbol{\mu}_{Z}^{(j+1)}\right)$, we can perform the conventional MPP-search methods (Rackwitz and Flessler 1978; Schittkowski 1986) to solve the following optimization to obtain the new MPP $\mathbf{u}_{\mathrm{MPP}}^{(j+1)}(t_i)$ in the $(j+1)-$th iteration:

$$\begin{aligned} &\min \quad \|\mathbf{u}\| \\ &\text{s. t.} \quad \widehat{G}_{t_i}\left(\mathbf{u}, \mathbf{d}^{(j+1)}, \boldsymbol{\mu}_{\mathbf{Z}}^{(j+1)}\right) = 0 \end{aligned} \tag{24}$$

However, it can be noticed that optimum $\mathbf{u}_{\mathrm{MPP}}^{(j+1)}(t_i)$ of (24) is actually the least-norm solution of the undetermined equation:

$$k\left[\mathbf{u}_{\mathrm{MPP}}^{(j)}(t_i)\right]^T\mathbf{u} = k\beta^2 - \left[\mathbf{A}^T\mathbf{B}^T\right] \bullet \begin{bmatrix} \Delta\mathbf{d}^{(j+1)} \\ \Delta\boldsymbol{\mu}_{\mathrm{Z}}^{(j+1)} \end{bmatrix} \tag{25}$$

Therefore, there is no need to perform the MPP-search process, we can directly derive the analytic expression of $\boldsymbol{u}_{MPP}^{(j+1)}(t_i)$ with the least-square method as

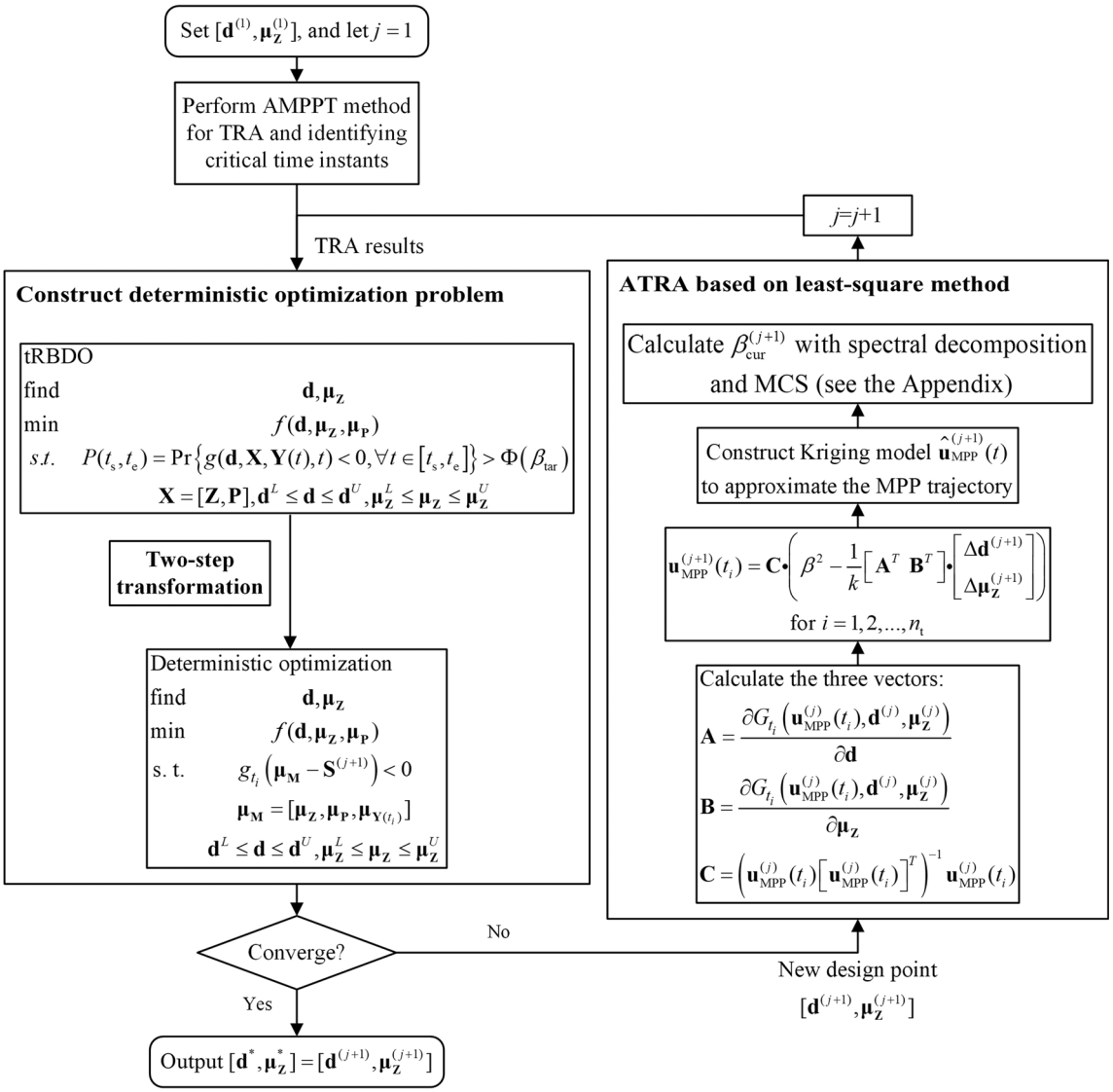

Fig. 3 Flowchart of the proposed SATO method

$$\mathbf{u}_{\mathrm{MPP}}^{(j+1)}(t_i)\approx\mathbf{C}\cdot\left(\beta^2-\frac{1}{k}\left[\mathbf{A}^T\boldsymbol{B}^T\right]\cdot\begin{bmatrix}\Delta\mathbf{d}^{(j+1)}\\ \Delta\boldsymbol{\mu}_{\mathrm{Z}}^{(j+1)}\end{bmatrix}\right)$$
$$\mathbf{C}=\left(\mathbf{u}_{\mathrm{MPP}}^{(j)}(t_i)\left[\mathbf{u}_{\mathrm{MPP}}^{j}(t_i)\right]^T\right)^{-1}\mathbf{u}_{\mathrm{MPP}}^{(j)}(t_i)\tag{26}$$

Similarly, for each time instant $t_i(i=1,2,..,n_t)$, we can derive $\mathbf{u}_{\mathrm{MPP}}^{(j+1)}(t_i)$ with (26), and obtain a new group of "time-MPP" pairs $\left\{\left(t_i,\mathbf{u}_{\mathrm{MPP}}^{(j+1)}(t_i)\right)|i=1,21,..n_t\right\}$. Then, with these samples, a Kriging model $\hat{\mathbf{u}}_{\mathrm{MPP}}^{(j+1)}(t)$ for the MPP trajectory can be constructed. Finally, the time-variant reliability index $\beta_{cur}^{(j+1)}$ at the new design point $\left[\mathbf{d}^{(j+1)},\boldsymbol{\mu}_{\mathrm{Z}}^{(j+1)}\right]$ can be calculated with the MPP trajectory $\hat{\mathbf{u}}_{\mathrm{MPP}}^{(j+1)}(t)$ (see the Appendix).

3.2.2 Some remarks

First, compare computational complexities of the proposed ATRA method with the AMPPT method.

For the proposed ATRA method, the computational cost mainly comes from calculating the partial derivatives **A** and **B** in (21) with the numerical method. Therefore, the number of function evaluations (FEs) required by the proposed ATRA can be calculated by

$$FE_{\mathrm{ATRA}}=(n_d+n_z)n_t\tag{27}$$

For the AMPPT method, the computational cost mainly comes from performing n_t MPP-searches at $t_i(i=1,2,\ldots,n_t)$. In practice, efficient gradient-based algorithms are commonly used to perform the MPP-searches, such as Sequential Quadratic Programming (SQP) and Hasofer-Lind Rackwitz-

Fissler (HL-RF) algorithm (Rackwitz and Flessler 1978). Let the average number of iterations required by each MPP-search be n_{AVG} . Then, the number of FEs required by the AMPPT can be calculated by

$$FE_{\mathrm{AMPPT}} = \left(n_z + n_p + n_Y + 1\right) n_{\mathrm{AVG}} n_{\mathrm{t}} \tag{28}$$

The ratio of the computational complexities of ATRA to AMPPT can be calculated by

$$\frac{FE_{ATRA}}{FE_{AMPPT}} = \frac{n_d + n_z}{\left(n_z + n_p + n_Y + 1\right) n_{\mathrm{AVG}}} \tag{29}$$

In practice, each MPP-search generally requires dozens of iterations on average for convergence. Therefore, the ratioFE_{ATRA}/FE_{AMPPT} is generally far less than 1, and the proposed ATRA method can significantly reduce the computational cost of TRA.

Second, similar to other first-order Taylor expansion-based methods (Cheng et al. 2006; Zou and Mahadevan 2006; Yi et al. 2016), the proposed ATRA method may inevitably introduce some error relative to AMPPT in the first few iterations. However, as the design point series $\left\{\left[\mathbf{d}^{(j+1)}, \boldsymbol{\mu}_{\mathrm{z}}^{(j+1)}\right] | j = 1, 2, ..\right\}$ converge, the vector $\begin{bmatrix} \Delta\mathbf{d}^{(j+1)} \\ \Delta\boldsymbol{\mu}_{\mathrm{Z}}^{(j+1)} \end{bmatrix}$ in (26) tend to zero, and the error introduced by the ATRA method can also be reduced to zero. Generally, the proposed ATRA method takes only a few iterations to achieve an acceptable accuracy in practice, which is also demonstrated in the validation and application section of this paper.

3.3 Complete procedure

The flowchart of the proposed SATO method is shown in Fig. 3. First, the AMPPT method is performed to identify the critical time instants and the corresponding MPPs. Then, the two-step transformation is employed to convert the original tRBDO problem into a deterministic optimization problem to update the design point. Afterwards, the proposed ATRA method is performed to calculate the time-variant reliability at the new design point. Then, the two sub-procedures, deterministic optimization and ATRA, are performed sequentially until the convergence criterion is satisfied.

The proposed SATO method decouples the double-loop nested procedure in the original tRBDO into a sequential process of the two easy-to-solve sub-procedures, which can significantly improve the efficiency of tRBDO.

4 Validation and application

This section presents the validation and application of the proposed SATO method. First, a complicated welded beam problem is employed to verify the accuracy and efficiency of the proposed method, in comparison with the double-loop method (DLM) and the EMPP method proposed by Fang et al. (Fang et al. 2019). Then, the proposed SATO method is applied in a rocket inter-stage structure problem to show its capability in solving practical engineering problems.

4.1 Validation of the proposed method

4.1.1 Problem description

The welded beam problem is a complicated highly nonlinear tRBDO problem with 11 random variables/stochastic process and 3 types of reliability constraints, i.e., static reliability constraint, stationary time-variant reliability constraints, and nonstationary time-variant reliability constraints, and is commonly used to verify the effectiveness of tRBDO methods (Fang et al. 2019).

The welded beam is depicted in Fig. 4. The left end is fixed by welding, and the right end is subjected to a stochastic load $F(t)$. The depth Z_1 and length Z_2 of the welding point, and the

Table 1 Probabilistic characteristics of the variables in the welded beam

Variable	Distribution	Mean	Standard deviation	Autocorrelation coefficient function
Z_1	Normal	μ_{Z1}	0.2 mm	NA
Z_2	Normal	μ_{Z2}	2 mm	NA
Z_3	Normal	μ_{Z3}	2 mm	NA
Z_4	Normal	μ_{Z4}	0.2 mm	NA
σ	Normal	206.85 MPa	20.685 MPa	NA
L	Normal	355.6 mm	35.56 mm	NA
E	Normal	206850 MPa	20685 MPa	NA
G	Normal	82740 MPa	8274 MPa	NA
d_0	Normal	6.35 mm	0.635 mm	NA
τ	Normal	93.77 MPa	9.377 MPa	NA
$F(t)$	Gaussian process	26688 N	2668.8 N	$\exp(-\Delta t^2)$

height Z_3 and thickness Z_4 of the beam are considered as random design variables. The random parameters include the Young's Modulus E, the shear modulus G, the length of the beam L, the allowable displacement d_0 of the free end, the maximum shear stress τ, and maximum normal stress σ. The probabilistic characteristics of all involved variables are listed in Table 1.

The objective of this problem is to minimize the cost of welding, and the tRBDO problem is formulated as

$$\begin{aligned}
\min \quad & f(\boldsymbol{\mu}_{\mathbf{Z}}, \boldsymbol{\mu}_{\mathbf{p}}) = c_1 \mu_{Z_1}^2 \mu_{Z_2} + c_2 \mu_{Z_3} \mu_{Z_4} (\mu_L + \mu_{Z_2}) \\
\text{s. t.} \quad & \Pr\{g_i(\mathbf{X}, Y(t), t) < 0, \forall t \in [0, T]\} > \Phi(\beta_i^{target}), i = 1, 2, 3, 4, 5 \\
& \Pr\{g_3(\mathbf{X}) < 0\} > \Phi(\beta_3^{target}) \\
& g_1(\mathbf{X}, \mathrm{Y}(t), t) = \frac{\tau(\mathbf{X}, Y(t))}{\tau^*} - 1 \qquad g_2(\mathbf{X}, Y(t), t) = \frac{\sigma(\mathbf{X}, Y(t))}{\sigma^*} - 1 \\
& g_3(\mathbf{X}) = \frac{Z_1}{Z_4} - 1 \qquad g_4(\mathbf{X}, Y(t)t) = \frac{\delta(\mathbf{X}, Y(t))}{d_0} - 1 \\
& g_5(\mathbf{X}, Y(t)) = 1 - \frac{P_c(\boldsymbol{X})}{F(t)} \qquad \beta_i^{\text{target}} = 2.0, i = 1, 2, \ldots, 5 \\
& \boldsymbol{Z} = [Z_1, Z_2, Z_3, Z_4] \quad \mathbf{P} = [\sigma, L, E, G, d_0, \tau] \qquad \mathbf{X} = [\mathbf{Z}, \mathbf{P}] \quad Y(t) = F(t) \\
& 3.175\text{mm} < \mu_{z_1} < 50.8 \text{ mm} \qquad 0\text{mm} < \mu_{Z_2} < 254 \text{ mm} \\
& 0 \text{ mm} < \mu_{z_3} < 254 \text{ mm} \qquad 0 \text{ mm} < \mu_{z_4} < 50.8\text{mm} \\
& T = 10 \text{ years}
\end{aligned} \tag{30}$$

where

$$\begin{aligned}
& \tau(\boldsymbol{X}, Y(t)) = \sqrt{L(\mathbf{X}, Y(t))^2 + \frac{L(\boldsymbol{X}, Y(t)) S(\boldsymbol{X}, Y(t))^2}{R(\mathbf{X})} + S(\boldsymbol{X}, Y(t))^2} \\
& \sigma(\mathbf{X}, Y(t)) = \frac{6F(t)L}{Z_3^2 Z_4} \qquad \delta(\mathbf{X}, Y(t)) = \frac{4F(t)L^3}{EZ_3^3 Z_4} \\
& L(\mathbf{X}, Y(t)) = \frac{F(t)}{\sqrt{2}Z_1 Z_2} \qquad S(\boldsymbol{X}, Y(t)) = \frac{M(\boldsymbol{X}, Y(t)) R(\boldsymbol{X})}{J(\boldsymbol{X})} \\
& J(\boldsymbol{X}) = \sqrt{2Z_1 Z_2 \left[\frac{Z_2^2}{12} + \frac{(Z_1 + Z_3)^2}{4}\right]} \qquad P_c(\boldsymbol{X}) = \frac{4.013 Z_3 Z_4^3 \sqrt{EG}}{6L^2} \left(1 - \frac{Z_3}{4L}\sqrt{\frac{E}{G}}\right) \\
& \tau^* = \tau e^{-0.012t} \qquad \sigma^* = \sigma e^{-0.01t} \\
& C_1 = 6.74135 \times 10^{-5} \qquad C_2 = 2.93585 \times 10^{-6}
\end{aligned} \tag{31}$$

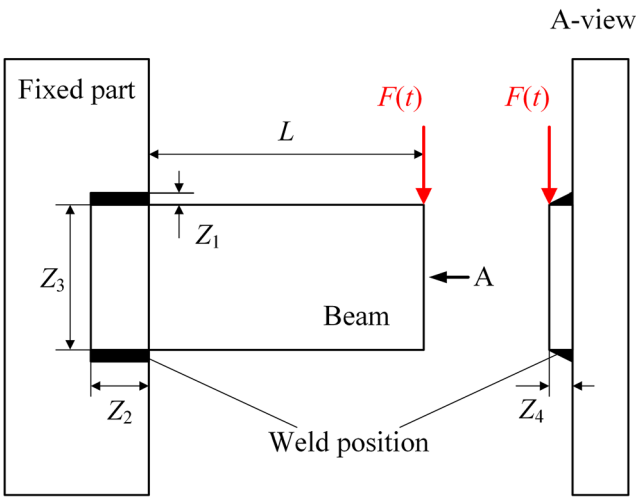

Fig. 4 The welded beam

4.1.2 Results and discussions

The deterministic optimization counterpart of the original tRBDO problem is firstly solved, and its optimum [6.2068, 157.9224, 210.5967, 6.2068] is used as the initial design point of the tRBDO methods. The DLM, EMPP, and SATO take 48, 5, and 5 iterations for convergence, respectively. The optimal solutions obtained by the three methods are listed in Table 2. The computational costs of the three methods are listed in Table 3, where FE_{total} denotes the total number of FEs, and FE_{TRA} denotes the number of FEs used for TRA, including both AMPPT and ATRA.

First, consider the accuracy of different tRBDO methods. It can be seen from Table 2 that the three methods almost find

Table 2 Optimal solutions of different tRBDO methods in the welded beam

Methods	Optimum	Objective	Reliability index
DLM	[6.6811, 227.4071, 254.0000, 7.2468]	3.8348	[2.0011, 2.0102, 2.0005, Inf, 2.1573]
EMPP	[6.6835, 227.2151, 254.0000, 7.2492]	3.8348	[1.9961, 2.0074, 2.0013, Inf, 2.1653]
SATO	[6.6873, 227.3335, 254.0000, 7.2530]	3.8382	[2.0027, 2.0109, 2.0019, Inf, 2.1722]

Table 3 Computational costs of different tRBDO methods in the welded beam

Methods	Iterations	AMPPT invocations	ATRA invocations	FE_{total}	FE_{TRA}
DLM	48	984	0	482,969	470,069
EMPP	5	20	0	11,516	6236
SATO	5	**4**	16	**4782**	**1084**

the same optimal solution, which demonstrates that all the three methods can effectively solve this problem.

Second, further analyze the accuracy of the proposed ATRA method in each iteration of SATO. Figure 5 presents the maximum mean square error (MSE) $\max_{t\in[0,T]} \sum_{j=1}^{n+m} \frac{\sigma_j^2(t)}{n} n+m$ of $\widehat{\mathbf{u}}_{\text{MPP}(t)}$ (see (46) in Appendix B) in each iteration of SATO. It can be seen that the maximum MSE of the Kriging models $\widehat{\mathbf{u}}_{\text{MPP}(t)}$ are always far less than 10^{-5}, which indicates that the Kriging models are accurate enough. Moreover, we also performed the AMPPT method after each ATRA invocation to calculate the accurate time-variant reliability index

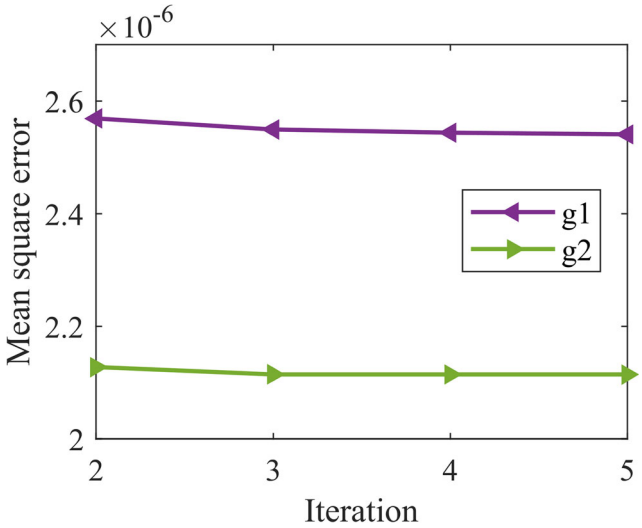

Fig. 5 Mean square error of the Kriging model in the proposed ATRA method

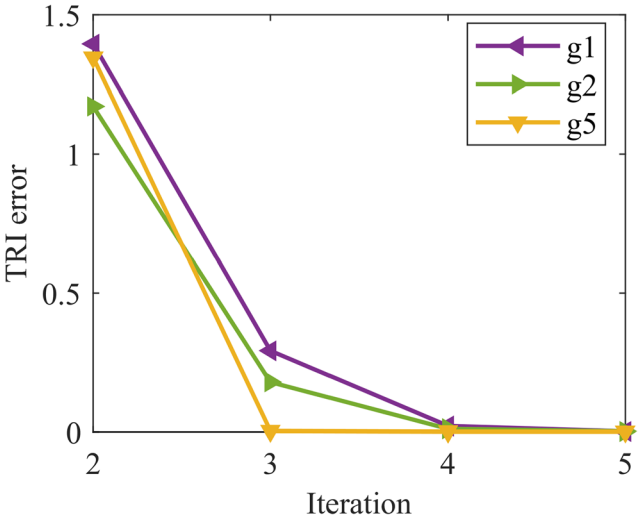

Fig. 6 TRI error of the proposed ATRA method in the welded beam

(TRI). The TRI error of the proposed ATRA relative to AMPPT is plotted in Fig. 6. Figure 6 only shows the TRI errors of g_1, g_2, and g_5, and this is because g_3 is a static reliability constraint and the TRI of g_4 is infinite. It is clear that in the second iteration, the TRI error of ATRA is relatively large. But only after two iterations, the TRI error is reduced to almost zero, which verifies the accuracy and robustness of the proposed ATRA method.

Third, compare the efficiency of the three tRBDO methods. It is clear from Table 3 that, due to the high nonlinearity of this problem, DLM takes 246 iterations and 482,969 FEs for convergence, and about 97% of the computational costs are used in the TRA. For more time-consuming simulation model is practical engineering, this computational burden is unaffordable. The convergence curves of EMPP and SATO are given in Fig. 7. From Table 3 and Fig. 7, it can be found that both EMPP and SATO need 5 iterations for convergence, but the FE_{total} of SATO is only 42.30% of that of EMPP, which

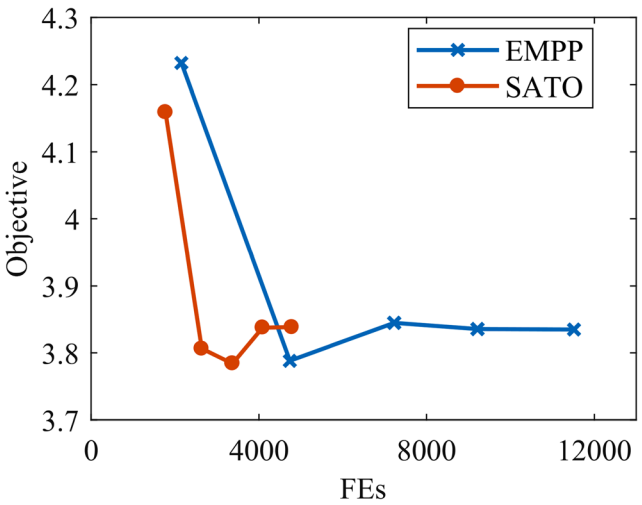

Fig. 7 Convergence curves of EMPP and SATO in the welded beam

verifies that the proposed SATO method is much more efficient than EMPP.

Fourth, further study the reason for the high efficiency of the proposed SATO. It can be seen from Table 3 that SATO significantly reduces the number of AMPPT invocations compared with EMPP (4 vs. 20). Figure 8 presents the number of FEs used for TRA (both AMPPT and ATRA) in each iteration of EMPP and SATO. This example includes four random design variables, two stationary time-variant reliability constraints, ($g_1$andg_2) and two nonstationary time-variant reliability constraints ($g_4$andg_5) The identified number of critical time instants for both $g_1$andg_2 are five. $g_4$andg_5 contains one critical time instant. Therefore, according to (27), the number of FFs used for TRA in each iteration is $12 \times 4 = 48$ It can be observed that each ATRA invocation takes less than 1/25 of the FEs required by each AMPPT invocation on average, which dramatically reduces the total computational cost of the proposed SATO method.

The above results and discussions verify that the proposed SATO method can significantly improve the efficiency of tRBDO while maintaining similar accuracy in comparison with DLM and EMPP.

4.2 Application in a rocket inter-stage structure

4.2.1 Problem description

In this subsection, the proposed SATO method is applied in the tRBDO problem of an inter-stage structure.

The stiffened cylindrical shell structure is a common structure form in the inter-stage structure of large launch vehicles. Figure 9 shows the finite element model of an inter-stage structure. The height of the inter-stage structure is 720 mm, and the diameter is 2300 mm. The inter-stage structure contains 72 axial frames and 10 ring frames. All the frames have a rectangular cross-section, as shown in Fig. 10a. There are 4 elliptical holes with the same shape on the wall of the structure, and the schematic diagram of the elliptical hole is shown in Fig. 10b. The upper end of the structure is subjected to a dynamic axial load (t), and the lower end is under fixed-supported constraints. The material properties of the structure are listed in Table 4.

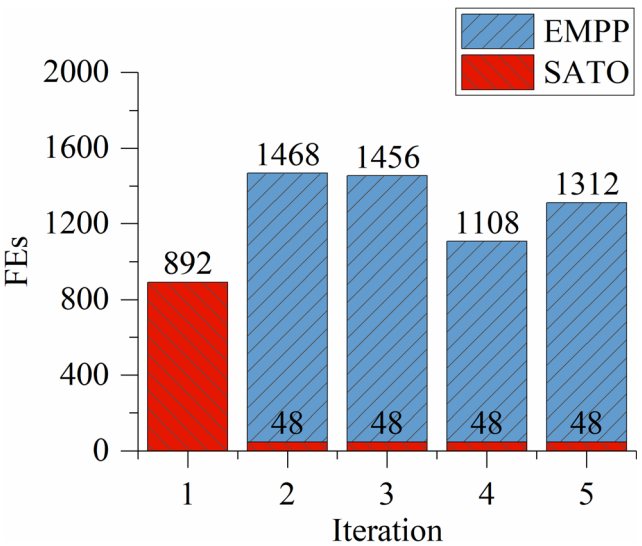

Fig. 8 The number of FFs used for TRA in each iteration of EMPP and SATO

This problem contains 5 random design variables, i.e., thickness of the wall T, thickness of the ring frames C_1, thickness of the axial frames C_2, and the lengths of the semi-major and semi-minor axes of the 4 elliptical holes A and B. The height of the ring and axial frames H is considered a random parameter. The probabilistic characteristics of all involved variables are given in Table 5.

During the flight time, the engine thrust of the rocket can be roughly considered as a constant. With the fuel consumption, the mass of the launch vehicle gradually decreases. Therefore, the axial load on the inter-stage structure gradually increases with time. In this paper, we model the dynamic axial load F(t) as a non-stationary stochastic process, and its mean, standard deviation, and autocorrelation coefficient functions are expressed as

$$\begin{aligned} \mu_F(t) &= 1000(t/160)^{1.5} + 1600\text{kN} \\ \sigma_F(t) &= 30\text{kN} \\ \rho_F(t_1,t_2) &= \exp(-(t_1-t_2))^2/100 \end{aligned} \tag{32}$$

The objective of this problem is to minimize the mass of the structure. The inter-stage structure fails if the maximum von Mises stress exceeds the yield strength $\sigma_y = 213.8$ MPa or axial displacement of the upper end of the structure exceeds $S_{\text{limit}} = 0.6$ mm during the flight time of 120 s. Therefore, the tRBDO problem can be expressed as:

$$\begin{aligned} \min \quad & f(\boldsymbol{\mu}_z, \mu_H) = m(\mu_T, \mu_C, \mu_{C_2}, \mu_A, \mu_B, \mu_H) \\ \text{s. t.} \quad & \Pr\{g_i(\boldsymbol{Z}, H, F(t)) < 0, \forall t \in [0,T]\} > \Phi(3.0), i = 1,2 \\ & g_i(\boldsymbol{Z}, H, F(t)) = \sigma_v(T, C_1, C_2, A, B, H, F(t)) - \sigma_y \\ & g_2(\boldsymbol{Z}, H, F(t)) = s(T, C_1, C_2, A, B, H, F(t)) - s_{\text{limit}} \\ & \boldsymbol{Z} = [T, C_1, C_2, A, B] \quad 4\text{mm} < \mu_T < 10\text{mm} \\ & 4\text{mm} < \mu_{c_1}, \mu_{c_2} < 15\text{mm} \quad 150\text{ mm} < \mu_A, \mu_B < 220\text{mm} \\ & T = 120\text{ s} \end{aligned} \tag{33}$$

Table 4 Material properties of the inter-stage structure

Modulus of elasticity	Density	Yield strength	Poisson's ratio
68,646 MPa	2700 kg/m^3	313.8 MPa	0.3

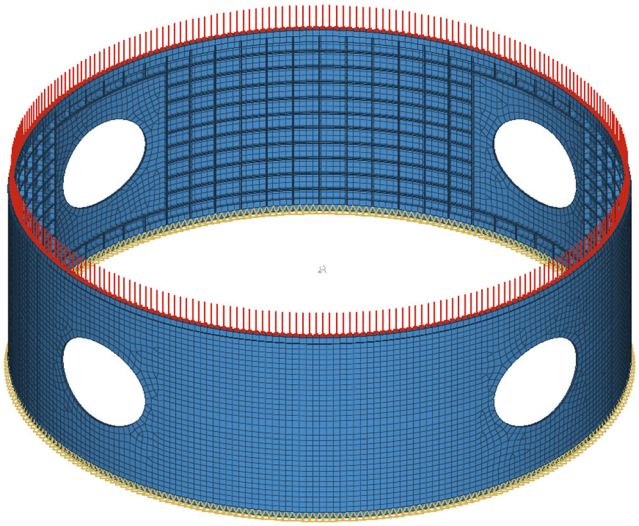

Fig. 9 Finite element model of the inter-stage structure

where $m(\bullet)$, $\sigma_v(\bullet)$, and $s(\bullet)$ are the mass, the maximum von Mises stress, and the maximum axial displacement of the structure, respectively.

In this paper, the CATIA software is used to build the parametric model of the inter-stage structure. Then, HyperMesh is employed to automatically generate the finite element mesh. Finally, Nastran is used for finite element analysis to calculate $m(\bullet)$, $\sigma_v(\bullet)$, and $s(\bullet)$.

4.2.2 Results and discussions

First, solve the deterministic optimization counterpart of the original tRBDO problem in (33) without considering the uncertainties. The resulting optimum is listed in Table 6. It can be seen that the optimal mass is 137.67 kg, and both the stress and displacement constraints are satisfied. However, when the static and time-variant uncertainties are taken into account, the TRIs of g_1 and g_2 are only 0.7534 and 0.0013, respectively, far from meeting the TRI requirement of 3.0. This result indicates

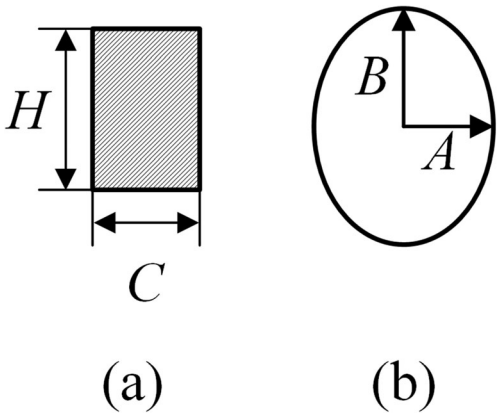

Fig. 10 Schematic diagrams of the rectangular frame and the elliptical holes

Table 5 Probabilistic characteristics of the variables of the inter-stage structure

Variable	Distribution	Mean	Standard deviation	Autocorrelation coefficient function
T	Normal	μ_T	0.6 mm	NA
C_1	Normal	μ_{C1}	0.6 mm	NA
C_2	Normal	μ_{C2}	0.6 mm	NA
A	Normal	μ_A	0.6 mm	NA
B	Normal	μ_B	0.6 mm	NA
H	Normal	15 mm	0.6 mm	NA
$F(t)$	Gaussian process	$\mu_F(t)$	$\sigma_F(t)$	$\rho_F(t_1,t_2)$

that it may lead to huge risk if the inter-stage structure is designed according to the deterministic optimum.

Second, use the deterministic optimum in Table 6 as initial design point, and perform EMPP and SATO to solve the original tRBDO problem. The resulting optima are listed in Table 7. It is found that the optimum of the proposed SATO method is very close to that of EMPP, which verifies the effectiveness and accuracy of the proposed method.

Third, compare the deterministic and tRBDO optima. Figure 11 shows the von Mises stress contours and axial displacement contours of the two optima. It is obvious that the tRBDO optimum considerably reduces the maximum von Mises stress and axial displacement. Compare Tables 6 and 7, it can be seen that although the tRBDO optimum increases the mass of the inter-stage (from 137.67 to 162.80 kg), the TRIs of g_1 and g_2 are also significantly increased and meet the TRI requirement. This result demonstrates that, in practical applications, the tRBDO optimum are much more reliable than the deterministic optimum.

Fourth, compare the efficiency of EMPP and SATO. Table 8 lists the detailed computational costs of EMPP and SATO. It should be noted that in this example, a single finite element analysis (FEA) can simultaneously calculate the weight, the maximum von Mises stress, and the maximum axial displacement of the structure. Therefore, the last two columns of Table 8 (FEA_{total} and FEA_{TRA}) are the number of FEAs, instead of the number of FEs. Figure 12 shows the

Table 6 Deterministic optimum of the inter-stage structure

Parameters	Value
Deterministic optimum	[6.02, 14.98, 4.09, 150.04, 219.98] mm
Mass	137.67 kg
Max von Mises stress	195.81 MPa
Max axial displacement	0.60 mm
TRI of g_1	0.7534
TRI of g_2	0.0013

Table 7 tRBDO optima of the inter-stage structure

Methods	Optimum	Mass (kg)	TRI
EMPP	[7.84, 15.00, 4.00, 150.00, 192.81]	162.76	[3.4895, 2.9983]
SATO	[7.85, 15.00, 4.00, 150.00, 192.76]	162.80	[3.5426, 3.0091]

convergence curves of EMPP and SATO. It can be seen that although SATO takes two more iteration for convergence than EMPP, the FE_{total} of SATO is only 47.31% of that of EMPP.

Additionally, further study the reason for the high efficiency of SATO. It can be observed from Table 8 that, in comparison with EMPP, the computation cost reduction (980 FEs) of SATO mainly comes from the computation cost reduction in TRA (672 FEs). Figure 13 shows the number of FFs used for TRA in each iteration of EMPP and SATO. This example includes five random design variables and two time-variant reliability constraints. The number of critical time instants identified by AMPPT for both time-variant reliability constraints are five. Therefore, according to (27), the number of FFs used for TRA in each iteration is $10 \times 5 = 50$. It is clear that the number of FFs of each ATRA invocation is only about 1/9 of that of each AMPPT invocation. Therefore, the total computational cost of the proposed SATO method is significantly reduced in comparison with EMPP.

These results and discussions demonstrate the effectiveness and efficiency of the proposed SATO in solving the practical engineering problem.

5 Conclusions

This paper proposes a novel decoupled SATO method to improve the efficiency of tRBDO. First, a two-step method is

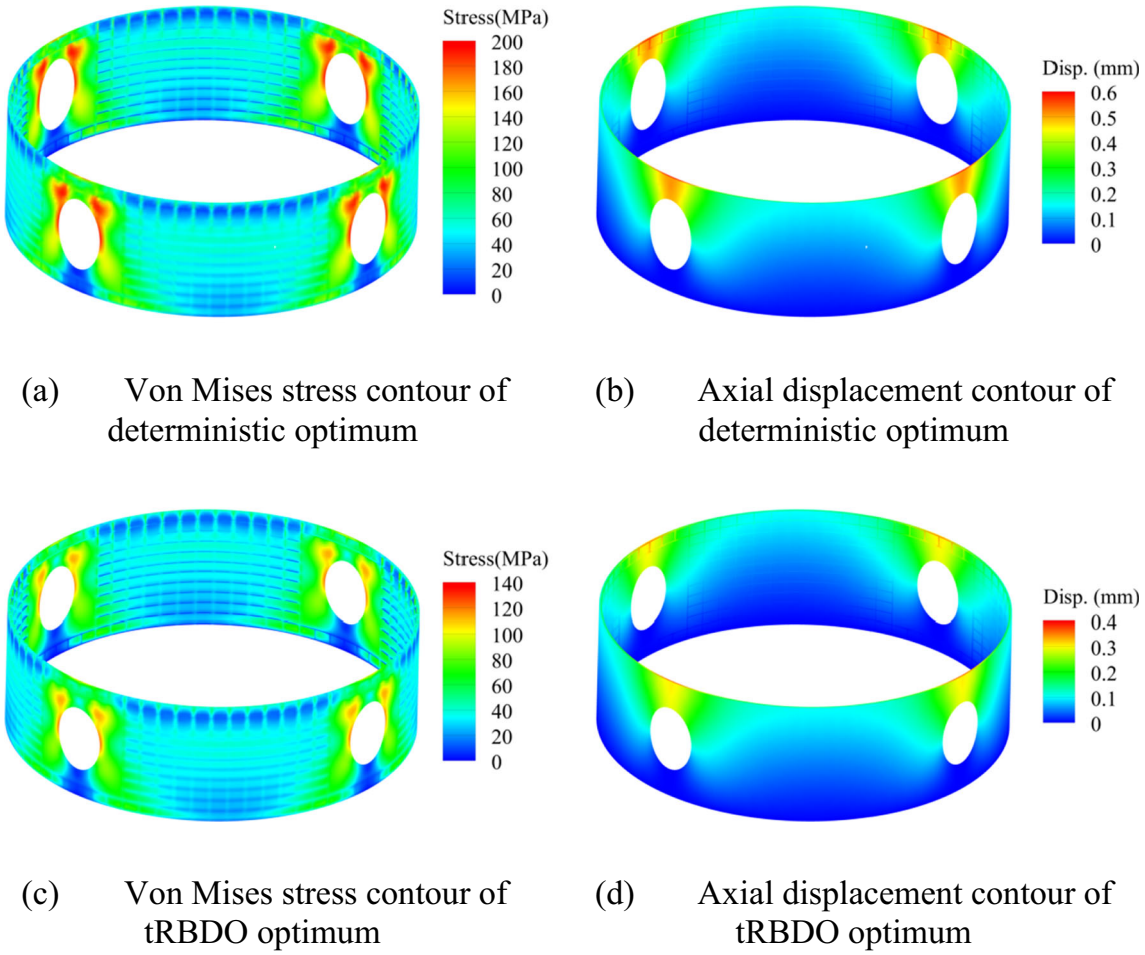

(a) Von Mises stress contour of deterministic optimum

(b) Axial displacement contour of deterministic optimum

(c) Von Mises stress contour of tRBDO optimum

(d) Axial displacement contour of tRBDO optimum

Fig. 11 Comparison of deterministic optimum and tRBDO optimum of the inter-stage structure. **a** Von Mises stress contour of deterministic optimum. **b** Axial displacement contour of deterministic optimum. **c** Von Mises stress contour of tRBDO optimum. **d** Axial displacement contour of tRBDO optimum

Table 8 Computational costs of EMPP and SATO in the inter-stage structure

Methods	Iterations	AMPPT invocations	ATRA invocations	FEA_{total}	FEA_{TRA}
EMPP	3	6	0	1860	1308
SATO	5	**2**	8	**880**	**636**

proposed to directly transform the original tRBDO problem into an equivalent deterministic optimization problem. Second, a novel ATRA method is proposed, which employs the least-square method to calculate the MPPs and therefore can notably reduce the computational cost for the TRA. As a result, the proposed SATO method decouples the nested double-loop procedure in tRBDO into a sequential process of the two sub-procedures: ATRA and deterministic optimization.

Test results of the welded beam problem verify that the proposed SATO method can achieve similar accuracy to the compared methods, while considerably reducing the computational cost. The rocket inter-stage problem shows that the proposed method can be applied into practical engineering problems to improve the reliability of engineering structures under time-variant uncertainties.

Like other first-order Taylor expansion-based methods, the proposed method may produce large error if the time-variant performance function of the tRBDO problem is highly nonlinear. To address this problem, the second-order reliability method (SORM) can be performed at the critical time instants to achieve higher accuracy in future studies.

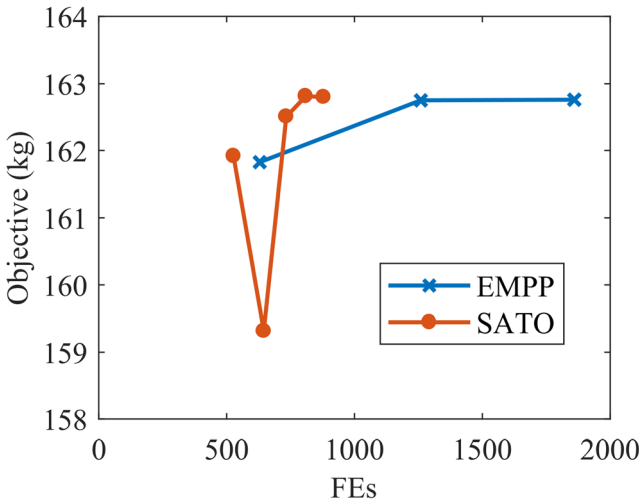

Fig. 12 Convergence curves of EMPP and SATO in the inter-stage structure

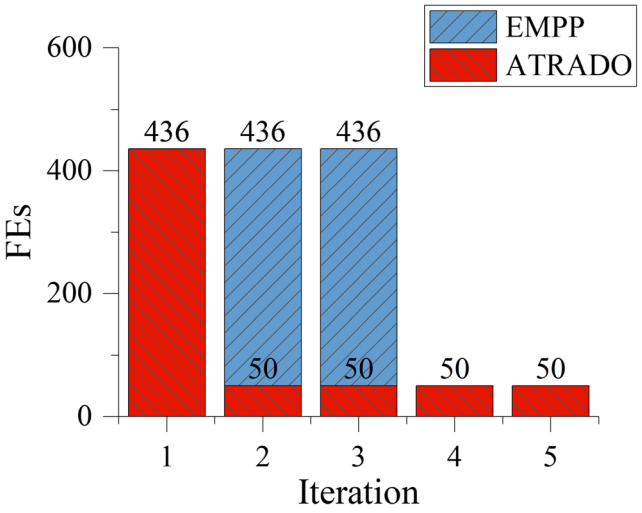

Fig. 13 The number of FFs used for TRA in each iteration of EMPP and SATO

Appendix 1

AMPPT method for TRA and identifying critical time instants

The AMPPT method is based on the concept of MPP trajectory (Zhang et al. 2021). It can not only accurately calculate the time-variant reliability, but also identify the critical time instants within the time interval $[0, T]$ via an adaptive sampling process.

For an arbitrary time instant $t_a \in [0, T]$, denote the MPP of the instantaneous performance function $g(\mathbf{d}, \mathbf{X}, \mathbf{Y}(t_a), t_a)$ as $\mathbf{u}_{MPP}(t_a)$. When t_a varies from 0 to T, the MPP $\mathbf{u}_{MPP}(t_a)$ will move from $\mathbf{u}_{MPP}(0)$ to $\mathbf{u}_{MPP}(T)$. If we connect all these MPPs, a curve $\mathbf{u}_{MPP}(t)(t \in [0, T])$ in u-space can be obtained, which is defined as the MPP trajectory. Figure 14 shows a schematic diagram of the MPP trajectory, where the solid curves represent the limit-state boundaries at the critical time instants.

For a given TRA problem, the AMPPT method first approximates its MPP trajectory with the adaptive Kriging model $\hat{\mathbf{u}}_{MPP}(t)$, and then calculates the time-variant reliability

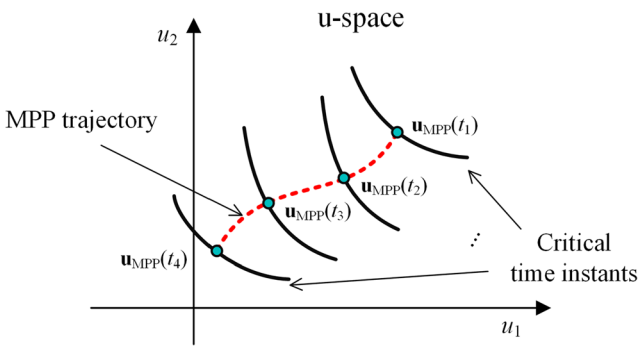

Fig. 14 Schematic diagram of the MPP trajectory and critical time instants

based on $\widehat{\mathbf{u}}_{\mathrm{MPP}}(t)$, The solution process of AMPPT consists of three steps, which are briefly described as follows.

First, discretize $[0, T]$ into N_{init} equidistant time instants, and perform MPP searches at these time instants to obtain the initial time-MPP samples. $\{(t_i, \mathbf{u}_{\mathrm{MPP}}(t_i))|\, i = 1, 2, .., N_{\mathrm{init}}\}$ Then, build a rough Kriging model $\widehat{\mathbf{u}}_{\mathrm{MPP}}(t)$ with these samples. Afterwards, perform an adaptive sampling process to iteratively identify the critical time instants t^*, at which the Kriging model $\widehat{\mathbf{u}}_{\mathrm{MPP}}(t)$ has the largest prediction variance,

$$t^* = \arg\max_{t\in[t_s,\, t_e]} \frac{\sum_{j=1}^{n+m}\sigma_j^2(t)}{n+m} \tag{34}$$

where $\sigma_j^2(t)$ $(j = 1, 2, \cdots n + m)$ is the prediction variance of the j-th component of $\widehat{\mathbf{u}}_{\mathrm{MPP}}(t)$. Then, perform MPP-search at t^* to obtain a new sample $(t^*, \mathbf{u}_{\mathrm{MPP}}(t^*))$, and update $\widehat{\mathbf{u}}_{\mathrm{MPP}}(t)$ accordingly. Repeat this process until the Kriging model $\widehat{\mathbf{u}}_{\mathrm{MPP}}(t)$ is accurate enough.

Second, according to $\widehat{\mathbf{u}}_{\mathrm{MPP}}(t)$, transform the response of the time-variant performance function $g(\mathbf{d}, \boldsymbol{X}, \boldsymbol{Y}, (t), t)$ into an equivalent Gaussian process $H(t)$. The mean, standard deviation, and autocorrelation coefficient functions of $H(t)$ are derived as:

$$\begin{aligned}
\mu(t) &= -\beta(t) = -\left\|\widehat{\mathbf{u}}_{\mathrm{MPP}}(t)\right\| \\
\sigma(t) &= 1 \\
\rho(t_1,t_2) &= \frac{\mathrm{Cov}(H(t_1),H(t_2))}{\sigma(t_1)\sigma(t_2)} \\
&= \mathrm{Cov}\left(-\beta(t_2) + (\boldsymbol{a}_{\mathrm{v}}(t_1))^T\mathbf{V} + (\boldsymbol{a}_{\mathrm{w}}(t_1))^T\mathbf{W}_1, -\beta(t_2) + \boldsymbol{a}_{\mathrm{v}}(t_2)\right)^T\mathbf{V} + \boldsymbol{a}_{\mathrm{w}}(t_1)\right)^T\mathbf{W}_2\Big) \\
&= \mathrm{Cov}\left(\left(\boldsymbol{a}_{\mathrm{v}}(t_1)\right)^T\mathbf{V} + (\boldsymbol{a}_{\mathrm{w}}(t_1))^T\mathbf{W}_1, (\boldsymbol{a}_{\mathrm{v}}(t_2))^T\mathbf{V} + (\boldsymbol{a}_{\mathrm{w}}(t_2))^T\mathrm{W}_2\right) \\
&= \mathrm{Cov}\left(\left(\boldsymbol{a}_{\mathrm{v}}(t_1)^T\mathbf{V}, \left(\boldsymbol{a}_{\mathrm{v}}\left(t_2\right)^T\mathbf{V}\right) + \mathrm{Cov}\left((\boldsymbol{a}_{\mathrm{w}}(t_1))^T\mathrm{W}_1, (\boldsymbol{a}_{\mathrm{w}}(t_2))^T\mathrm{W}_2\right)\right.\right. \\
&= (\boldsymbol{a}_{\mathrm{v}}(t_1))^T\boldsymbol{a}_{\mathrm{v}}(t_2) + (\boldsymbol{a}_{\mathrm{w}}(t_1))^T\mathbf{C}(t_1,t_2)\boldsymbol{a}_{\mathrm{w}}(t_2)
\end{aligned} \tag{35}$$

where $\mathbf{C}(t_1, t_2)$ is a $n_Y \times n_Y$ correlation coefficient matrix. $\mathbf{V}$ and $\mathbf{W}$ are independent standard normal random variables transformed from $\mathbf{X}$ and $\boldsymbol{Y}(t)$, respectively. $\boldsymbol{a}_{\mathrm{v}}(t)$ and $\boldsymbol{a}_{\mathrm{W}}(t)$ are calculated by

$$\begin{aligned}
\boldsymbol{\alpha}_{\mathrm{V}}(t) &= \widehat{\mathbf{u}}_{\mathrm{MPP,V}}(t)/\beta(t) \\
\boldsymbol{\alpha}_{\mathrm{W}}(t) &= \widehat{\mathbf{u}}_{\mathrm{MPP,W}}(t)/\beta(t) \\
\widehat{\mathbf{u}}_{\mathrm{MPP}}(t) &= \left[\widehat{\mathbf{u}}_{\mathrm{MPP,V}}(t), \widehat{\mathbf{u}}_{\mathrm{MPP,W}}(t)\right]
\end{aligned} \tag{36}$$

Finally, calculate the time-variant reliability based on spectral decomposition (Sudret and Der Kiureghian 2002) and Monte Carlo Simulation (MCS). Discretize the time interval $[0, T]$ into s equidistant time instants $t_i (i = 1, 2, \ldots, s)$, and construct a covariance matrix $\sum$ as

$$\boldsymbol{\Sigma} = \begin{bmatrix} \mathrm{Cov}(t_1,t_1) & \mathrm{Cov}(t_2,t_1) & \cdots & \mathrm{Cov}(t_s,t_1) \\ \mathrm{Cov}(t_1,t_2) & \mathrm{Cov}(t_2,t_2) & \cdots & \mathrm{Cov}(t_s,t_2) \\ \vdots & \vdots & \ddots & \vdots \\ \mathrm{Cov}(t_1,t_s) & \mathrm{Cov}(t_2,t_s) & \cdots & \mathrm{Cov}(t_s,t_s) \end{bmatrix}_{s\times s} \tag{37}$$

where, $Cov(t_i, t_j) = \sigma(t_i)\sigma(t_j)\rho(t_i, t_j)$, for $i, j = 1, 2, \cdots, s$. Then, $H(t)$ can be decomposed as (Sudret and Der Kiureghian 2002)

$$H(t) \approx \mu(t) + \sigma(t)\sum_{k=1}^{p}\frac{\xi_k}{\sqrt{\lambda_k}}\mathbf{Q}_k^T\boldsymbol{\rho}(t) \tag{38}$$

where $\xi_k (k = 1, 2, \ldots, p)$ are independent standard normal random variables;λ_k and $\mathbf{Q}_k$ are the eigenvalues and eigenvectors of $\sum$, respectively; $\boldsymbol{\rho}(t) = [\mathrm{Cov}(t_1, t), \mathrm{Cov}(t_2, t), .., \mathrm{Cov}(t_p, t)]^T$ is a covariance vector.

Use (38) to generate N_{MCS} samples $H^{(j)} = \left[h_1^{(j)}, h_2^{(j)}, \cdots, h_s^{(j)}\right]$, $(j = 1, 2, \cdots, N_{MCS})$ of $H(t)$, and the time-variant reliability index β_{cur} can be estimated by

$$\beta_{\mathrm{cur}} = \Phi^{-1}(P(T)) = \Phi^{-1}\left(\frac{\sum_{j=1}^{N_{\mathrm{MCS}}} I\left(H^{(i)}\right)}{N_{\mathrm{MCS}}}\right) \tag{39}$$

where $I(H^{(j)})$ is an indicator function. If $\max_{i=l}^{s}\left(h_i^{(j)}\right) < 0$, $I(H^{(j)}) = 1$; otherwise, $I(H^{(j)}) = 0$.

Appendix 2

Kriging model

In both the AMPPT method described above and the ATRA method proposed in Section 3.2, the Kriging model (Lophaven et al. 2002; Gano et al. 2006) is selected to approximate the MPP trajectory due to its advantage in providing the prediction variance and its successful applications in field of reliability analysis (Hawchar et al. 2018; Zhang et al. 2019; Li et al. 2020).

The Kriging model approximates the jth$(j = 1, 2, \ldots, n + m)$ component $\mu_{\mathrm{MPP},\,j}(t)$ of the MPP trajectory $\mathbf{u}_{\mathrm{MPP}}(t)$ (see Fig. 14) as

$$\widehat{u}_{\mathrm{MPP},j}(t) = f(t) + s(t) \tag{40}$$

where f(t) is a polynomial term of t and $s(t)$ is a Gaussian process with zero mean and covariance $\mathrm{Cov}[s(t_p), s(t_q)]$ In this paper,$f(t)$ is treated as a constant μ. The covariance $\mathrm{Cov}[s(t_p), s(t_q)]$ of $s(t)$ is calculated by

$$\mathrm{Cov}\left[s\left(t_p\right), s\left(t_q\right)\right] = \sigma^2 R\left(t_p, t_q\right) = \sigma^2\exp\left[-\theta\left(t_p - t_q\right)\right]^2 \tag{41}$$

where σ^2 is the variance of $s(t)$, $R(t_p, t_q)$ is the correlation coefficient, and θ is a parameter that can be determined by

the maximum likelihood estimation (Giunta and Watson 1998).

Assume the number of "time-MPP" pairs $\{(t_i, \boldsymbol{u}_{MPP}(t_i))_{\mathrm{L}} i = 1, 2, \cdots n\}$ is n. Denote $y = \{u_{MPP,j}(t_i)\}$. The natural logarithm of the likelihood function is defined as

$$L(\theta|\mathbf{y}) = -\frac{1}{2}\left[n\ln(2\pi) + n\ln\sigma^2 + \ln|\mathbf{R}| + \frac{(\mathbf{y}-\mathbf{A}\mu)^T\mathbf{R}^{-1}(\mathbf{y}-\mathbf{A}\mu)}{2\sigma^2}\right] \tag{42}$$

where $\mathbf{R} = [R(t_p, t_q)]_{n\times n}$ is a $n \times n$ correlation matrix and $\mathbf{A}$ is a $n \times 1$ unit vector. By setting the derivatives of (42) with respect to μ and σ^2 to zero, μ and σ^2can be estimated as

$$\widehat{\mu} = \frac{\mathbf{A}^T\mathbf{R}^{-1}\mathbf{y}}{\mathrm{A}^T\mathbf{R}^{-1}\mathbf{y}} \quad \widehat{\sigma}^2 = \frac{(\boldsymbol{y}-\mathbf{A}\mu)^T\mathbf{R}^{-1}(\mathbf{y}-\mathbf{A}\mu)}{n} \tag{43}$$

Substituting (43) into (42),θ can be determined by maximizing the likelihood function

$$\theta = \underset{\theta}{\operatorname{argmax}}\left(-\frac{n\ln\widehat{\sigma}^2 + \ln|\mathbf{R}|}{2}\right) \tag{44}$$

Once all hyper parameters are obtained, the Kriging model $\widehat{u}_{\mathrm{MPP},j}(t)$ can be used to predict the jth ($j = 1, 2, \ldots, n+m$) component of the MPP at an arbitrary time instant t:

$$\widehat{u}_{\mathrm{MPP},j}(t) = \widehat{\mu} + \mathbf{r}^T\mathbf{R}^{-1}\left(\mathbf{y}-\mathbf{A}\widehat{\mu}\right) \tag{45}$$

where $\mathbf{r}$ is a correlation vector defined by $\mathbf{r} = [R(t,t_1), R(t,t_2), \ldots, R(t,t_n)]^T$. The variance of the prediction in (45) is given by

$$\sigma_j^2(t) = \sigma^2\left[1-\boldsymbol{r}^T\mathbf{R}^{-1}\mathbf{r} + \frac{\left(1-\mathbf{A}^T\mathbf{R}^{-1}\mathbf{r}\right)^2}{\mathbf{A}^T\mathbf{R}^{-1}\mathbf{A}}\right] \tag{46}$$

Supplementary Information The online version contains supplementary material available at https://doi.org/10.1007/s00158-021-02999-9.

Acknowledgements The present work was partially supported by the National Natural Science Foundation of China (Grant No. 11502209), the National Defense Fundamental Research Funds of China (Grant No. JCKY2016204B102, JCKY2016208C001).

Declarations

Conflict of interest The authors declare that they have no conflict of interest.

Replication of results The core source code of the proposed method and the detailed results are provided in the supplementary material.

References

Agarwal H, Mozumder CK, Renaud JE, Watson LT (2007) An inverse-measure-based unilevel architecture for reliability-based design optimization. Struct Multidiscip Optim 33:217–227. https://doi.org/10.1007/s00158-006-0057-3

Cheng G, Xu L, Jiang L (2006) A sequential approximate programming strategy for reliability-based structural optimization. Comput Struct 84:1353–1367. https://doi.org/10.1016/j.compstruc.2006.03.006

Du X, Chen W (2004) Sequential Optimization and Reliability Assessment Method for Efficient Probabilistic Design. J Mech Des 126:225–233. https://doi.org/10.1115/1.1649968

Fang T, Jiang C, Huang Z et al (2019) Time-variant reliability-based design optimization using an equivalent most probable point. IEEE Trans Reliab 68:175–186. https://doi.org/10.1109/TR.2018.2823737

Gano SE, Renaud JE, Martin JD, Simpson TW (2006) Update strategies for kriging models used in variable fidelity optimization. Struct Multidiscip Optim 32:287–298. https://doi.org/10.1007/s00158-006-0025-y

Giunta A, Watson L (1998) A comparison of approximation modeling techniques - Polynomial versus interpolating models. In: 7th AIAA/USAF/NASA/ISSMO Symposium on Multidisciplinary Analysis and Optimization. American Institute of Aeronautics and Astronautics, Reston, Virigina

Hawchar L, El Soueidy C-P, Schoefs F (2018) Global kriging surrogate modeling for general time-variant reliability-based design optimization problems. Struct Multidiscip Optim 58:955–968. https://doi.org/10.1007/s00158-018-1938-y

Hu Z, Du X (2016) Reliability-based design optimization under stationary stochastic process loads. Eng Optim 48:1296–1312. https://doi.org/10.1080/0305215X.2015.1100956

Huang ZL, Jiang C, Zhou YS et al (2016) An incremental shifting vector approach for reliability-based design optimization. Struct Multidiscip Optim 53:523–543. https://doi.org/10.1007/s00158-015-1352-7

Huang ZL, Jiang C, Li XM et al (2017) A Single-Loop Approach for Time-Variant Reliability-Based Design Optimization. IEEE Trans Reliab 66:651–661. https://doi.org/10.1109/TR.2017.2703593

Jiang C, Fang T, Wang ZX et al (2017) A general solution framework for time-variant reliability based design optimization. Comput Methods Appl Mech Eng 323:330–352. https://doi.org/10.1016/j.cma.2017.04.029

Jiang C, Qiu H, Gao L et al (2020) Real-time estimation error-guided active learning Kriging method for time-dependent reliability analysis. Appl Math Model 77:82–98. https://doi.org/10.1016/j.apm.2019.06.035

Li M, Wang Z (2017) Sequential Kriging Optimization for Time-Variant Reliability-Based Design Involving Stochastic Processes. In: Volume 2A: 43rd Design Automation Conference. American Society of Mechanical Engineers

Li M, Wang Z (2018) Confidence-Driven Design Optimization Using Gaussian Process Metamodeling With Insufficient Data. J Mech Des 140:121405. https://doi.org/10.1115/1.4040985

Li F, Liu J, Wen G, Rong J (2019) Extending SORA method for reliability-based design optimization using probability and convex set mixed models. Struct Multidiscip Optim 59:1163–1179. https://doi.org/10.1007/s00158-018-2120-2

Li G, Yang H, Zhao G (2020) A new efficient decoupled reliability-based design optimization method with quantiles. Struct Multidiscip Optim 61:635–647. https://doi.org/10.1007/s00158-019-02384-7

Liang J, Mourelatos ZP, Tu J (2004) A Single-Loop Method for Reliability-Based Design Opteimization. In: Volume 1: 30th Design Automation Conference. ASMEDC, pp 419–430

Lim J, Lee B (2016) A semi-single-loop method using approximation of most probable point for reliability-based design optimization. Struct Multidiscip Optim 53:745–757. https://doi.org/10.1007/s00158-015-1351-8

Lophaven SN, Nielsen HB, Søndergaard J (2002) DACE-A MATLAB Kriging toolbox

Rackwitz R, Flessler B (1978) Structural reliability under combined random load sequences. Comput Struct 9:489–494. https://doi.org/10.1016/0045-7949(78)90046-9

Ren C, Xiong F, Mo B et al (2021) Design sensitivity analysis with polynomial chaos for robust optimization. Struct Multidiscip Optim 63:357–373. https://doi.org/10.1007/s00158-020-02704-2

Schittkowski K (1986) NLPQL: A fortran subroutine solving constrained nonlinear programming problems. Ann Oper Res 5:485–500. https://doi.org/10.1007/BF02739235

Schuëller GI, Jensen HA (2008) Computational methods in optimization considering uncertainties – An overview. Comput Methods Appl Mech Eng 198:2–13. https://doi.org/10.1016/j.cma.2008.05.004

Shi Y, Lu Z, Xu L, Zhou Y (2020) Novel decoupling method for time-dependent reliability-based design optimization. Struct Multidiscip Optim 61:507–524. https://doi.org/10.1007/s00158-019-02371-y

Sudret B, Der Kiureghian A (2002) Comparison of finite element reliability methods. Probabilistic Engineering Mechanics 17:337–348. https://doi.org/10.1016/S0266-8920(02)00031-0

Tu J, Choi KK, Park YH (1999) A New Study on Reliability-Based Design Optimization. J Mech Des 121:557–564. https://doi.org/10.1115/1.2829499

Wang Z, Wang P (2012) A Nested Extreme Response Surface Approach for RBDO With Time-Dependent Probabilistic Constraints. In: Volume 3: 38th Design Automation Conference, Parts A and B. American Society of Mechanical Engineers, pp 735–744

Wang P, Wang Z, Almaktoom AT (2014) Dynamic reliability-based robust design optimization with time-variant probabilistic constraints. Eng Optim 46:784–809. https://doi.org/10.1080/0305215X.2013.795561

Wang W, Gao H, Wei P, Zhou C (2017) Extending first-passage method to reliability sensitivity analysis of motion mechanisms. Proceedings of the Institution of Mechanical Engineers, Part O: Journal of Risk and Reliability 231:573–586. https://doi.org/10.1177/1748006X17717614

Wei P, Wang Y, Tang C (2017) Time-variant global reliability sensitivity analysis of structures with both input random variables and stochastic processes. Struct Multidiscip Optim 55:1883–1898. https://doi.org/10.1007/s00158-016-1598-8

Wu Y-T, Millwater HR, Cruse TA (1990) Advanced probabilistic structural analysis method for implicit performance functions. AIAA J 28:1663–1669. https://doi.org/10.2514/3.25266

Yi P, Cheng G (2008) Further study on efficiency of sequential approximate programming for probabilistic structural design optimization. Struct Multidiscip Optim 35:509–522. https://doi.org/10.1007/s00158-007-0120-8

Yi P, Zhu Z, Gong J (2016) An approximate sequential optimization and reliability assessment method for reliability-based design optimization. Struct Multidiscip Optim 54:1367–1378. https://doi.org/10.1007/s00158-016-1478-2

Yu S, Wang Z, Wang Z (2019) Time-Dependent Reliability-Based Robust Design Optimization Using Evolutionary Algorithm. ASCE-ASME J Risk and Uncert in Engrg Sys Part B Mech Engrg 5:. doi: https://doi.org/10.1115/1.4042921

Yu S, Zhang Y, Li Y, Wang Z (2020) Time-variant reliability analysis via approximation of the first-crossing PDF. Struct Multidiscip Optim 62:2653–2667. https://doi.org/10.1007/s00158-020-02635-y

Zafar T, Wang Z (2020) An efficient method for time-dependent reliability prediction using domain adaptation. Struct Multidiscip Optim 62:2323–2340. https://doi.org/10.1007/s00158-020-02707-z

Zafar T, Zhang Y, Wang Z (2020) An efficient Kriging based method for time-dependent reliability based robust design optimization via evolutionary algorithm. Comput Methods Appl Mech Eng 372:113386. https://doi.org/10.1016/j.cma.2020.113386

Zhang Y, Gong C, Fang H et al (2019) An efficient space division–based width optimization method for RBF network using fuzzy clustering algorithms. Struct Multidiscip Optim 60:461–480. https://doi.org/10.1007/s00158-019-02217-7

Zhang Y, Gong C, Li C (2021) Efficient time-variant reliability analysis through approximating the most probable point trajectory. Struct Multidiscip Optim 63:289–309. https://doi.org/10.1007/s00158-020-02696-z

Zou T, Mahadevan S (2006) A direct decoupling approach for efficient reliability-based design optimization. Struct Multidiscip Optim 31:190–200. https://doi.org/10.1007/s00158-005-0572-7